Journal of Geophysical Research: Solid Earth

RESEARCH ARTICLE
10.1029/2018JB015880

Special Section:
Gas Hydrate in Porous Media: Linking Laboratory and Field Scale Phenomena

The Effects of Hydrate on the Strength and Stiffness of Some Sands

B. N. Madhusudhan[1], C. R. I. Clayton[1], and J. A. Priest[2]

[1]Faculty of Engineering and Physical Sciences, University of Southampton, Southampton, UK, [2]Department of Civil Engineering, University of Calgary, Calgary, Alberta, Canada

Key Points:
- The effect of methane hydrate cement on the strength and stiffness of four different sands was determined from laboratory tests
- Measurements were made using very small strain probe tests during hydrate formation (using the excess gas method), and at failure
- Particle size, sphericity, and platyness have considerable and complex effects on the stiffness and strength of hydrate-bearing sediment

Supporting Information:
- Supporting Information S1
- Data Set S1

Correspondence to:
B. N. Madhusudhan,
mbnm1f13@soton.ac.uk

Citation:
Madhusudhan, B. N., Clayton, C. R. I., & Priest, J. A. (2019). The effects of hydrate on the strength and stiffness of some sands. *Journal of Geophysical Research: Solid Earth*, *124*. https://doi.org/10.1029/2018JB015880

Received 31 MAR 2018
Accepted 11 DEC 2018
Accepted article online 12 DEC 2018

Abstract Gas hydrates can form more or less at the same time as seafloor sediment. They can have the effect of significantly stiffening and strengthening deep-ocean sediments. Subsequent increases in situ temperature or decreases in pressure may trigger hydrate dissociation, leading to large reductions in the strength and stiffness of the sediment and possible seafloor instability. Gas hydrate dissociation not only removes cementing. It also releases freshwater and significant amounts of trapped gas that are dependent on multiple factors such as type of sediment, available pore space, hydrate morphology, and hydrate saturation. The presence of pock marks in areas of known seabed instability suggests that hydrate dissociation may have been a factor in triggering failure at these locations. Having reviewed the mechanisms by which the strength and stiffness of seabed sediment may be changed during dissociation, this paper reports the results of laboratory testing to evaluate the effects of loss of hydrate cement on strength and stiffness, for a range of sand-sized materials with differing particle size, specific surface area, and particle shape, using a laboratory gas hydrate triaxial apparatus. The results suggest that both the strength and the stiffness of hydrate-cemented granular materials are affected significantly by the specific surface available for hydrate cementation and, to a certain extent, by the particle shape. Uniform coarse granular sediments of lower specific surface area can suffer significant loss of stiffness and strength upon hydrate dissociation, changing the sediment from dilative to contractive. Finer-grained sediments appear less affected by dissociation.

1. Introduction

Naturally occurring gas hydrates are ice-like compounds that exist only under restricted thermobaric conditions, and where there is a biogenic or thermogenic source of methane. They are found in deep-ocean sediments, or in and below permafrost. Offshore, gas hydrate dissociation has been suggested as the possible trigger for a number of well-documented massive submarine slides, for example, at Storegga (Kvalstad et al., 2005; Talling et al., 2014), for the North Cascadian Slide (Yelisetti et al., 2014) and the Tuaheni Slope (Mountjoy et al., 2014), and for the AFEN slide (Madhusudhan et al., 2017). Thermobaric conditions at these locations certainly favor the creation of methane hydrates. Seafloor depths are between 200 and 1,200 m, while the headwall is between a few tens of meters to 150 m high, within the gas hydrate stability zone.

Dissociation of naturally occurring gas hydrate can be triggered by reduction in ambient pressure (e.g., as a result of changes in sea level) or by heating of the sediment (e.g., due to climate change or to thermal stimulation during exploitation). Knowledge of the amount of strength and stiffness lost during hydrate dissociation will be important when predicting and simulating the triggering and runout of submarine slope failures, and the identification of potential failure surfaces in sediments hosting gas hydrates.

2. Background

The loss of strength and stiffness of hydrate-bearing seafloor sediments as a result of dissociation will depend on the strength and stiffness of the hydrate itself, on the properties of the host sediment, and on the morphology of the hydrate. There are relatively few measurements of strength, and rather more of stiffness reported in the literature.

Song et al. (2010) found the compressive strength of solid methane hydrate at −5 °C to be 0.9 MPa under a 1-MPa confining pressure. For hydrate formed from ice/methane mixtures, at −5, −10, and −20 °C, under back pressures of 2.5, 5, and 10 MPa, Yu et al. (2011) measured unconfined compressive strengths of between 1.2 and 3 MPa. It can be seen from the above that solid hydrate has the strength of ice, similar to that of a weak

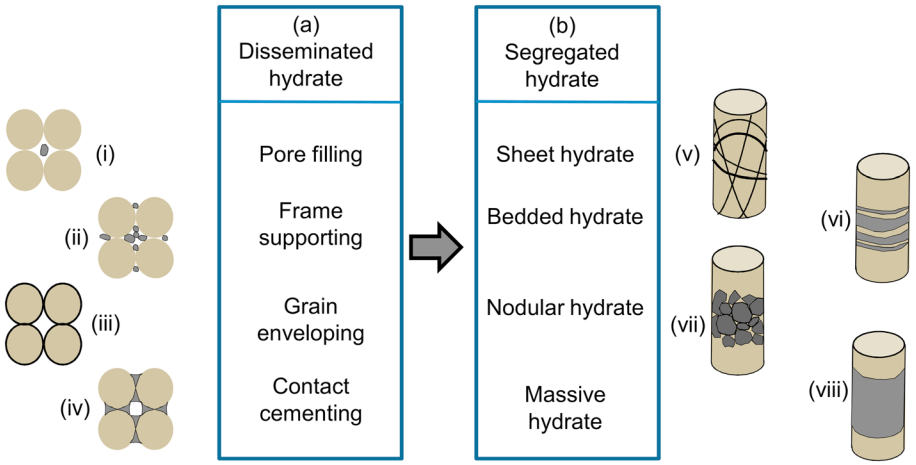

Figure 1. Deep-ocean hydrate morphologies (after Malone (1985), Dvorkin et al. (2000), and Rydzy (2014)).

rock. Hyodo et al. (2013) observed that the strength of hydrate-bearing Toyoura sands and silty sands obtained from the Nankai trough sediment increased exponentially with increase in methane hydrate saturation, and that peak strength was achieved at between 1 and 2% axial strain regardless of effective confining stress.

If isotropy and saturation can be assumed, the stiffness parameters (E and ν or G and K) of gas hydrate-bearing sediments are a simple function of its seismic wave velocity (Clayton, 2011). Stiffnesses at small strains are influenced mainly by hydrate content, morphology, and type of host sediments, rather than by effective stress (Clayton et al., 2010; Priest et al., 2005). Clayton et al. (2010) observed that the very small strain stiffness of hydrate-bearing sediments is strongly influenced by host sediment particle characteristics. For example, the stiffness of angular sand was more significantly affected by hydrate cementation than was the stiffness of rounded sand.

Hydrate will form whenever favorable thermobaric conditions exist, regardless of sediment type. However, the properties of the host sediment significantly influence the morphology of the hydrate. Fine-grained sediments suppress hydrate growth, forming veins only when gas fractures them. The proportion of void space filled in coarse, sandy, deposits (termed the "degree of hydrate saturation") depends upon there being sufficient methane gas, whether through in situ production of methane gas or a sustained upward migration of methane-saturated pore waters into the gas hydrate stability zone.

The properties of the host sediment significantly influence the morphology of the hydrate, and therefore the strength and stiffness once dissociation occurs. Under favorable conditions, hydrate acts to strengthen and stiffen submarine sediment. However, it is not uniformly distributed, and therefore, the strength increase during formation, and the loss of strength during dissociation, depends upon the way it is spread within the host sediment.

A wide range of hydrate morphologies has been observed to occur in nature (Figure 1). To some extent, these are controlled by the availability of methane. Limited quantities of methane gas, and hence disseminated hydrate, can be produced by the decomposition of in situ organic matter deposited within the pore space. However, much larger volumes of methane, migrating upward into the hydrate stability zone, will be required to produce the significant degrees of hydrate saturation associated with most segregated hydrate morphologies.

Disseminated hydrate morphologies (Figures 1(i)–1(iv)) occur in relatively permeable materials, such as sand. Experimental evidence on hydrate-bearing sands (Rees, 2009) suggests that at high saturations they can considerably stiffen the host sediment. In these sediments the hydrate is disseminated and nongrain-displacing. Pore-filling and frame-supporting hydrates (Figures 1(i) and 1(ii)) are considered to have little effect on the overall strength and stiffness properties of the sediment, until a significant proportion of the void space ($>$ 40%) in the host sediment becomes filled with hydrate. Because of the high specific surface area and

the hydrophilic nature of the sediment, grain enveloping hydrate (Figure 1(iii); Ecker et al., 1998; Rydzy, 2014) can similarly be expected to have relatively little effect on stiffness and strength.

This is in contrast with hydrate forming at contacts that leads to cementation (Figure 1(iv)), where only a few percent of the host sediment's pore space need be filled in order to produce a material that is strengthened significantly, and is insensitive to changes in effective stress (Clayton et al., 2005; Priest et al. 2005). In the laboratory, cementing at or around the grain-to-grain contacts has been produced using the "excess gas" method (Priest et al., 2005; Waite et al., 2004), whereas pore filling/frame supporting materials have been produced using the excess water method (Clayton et al., 2010; Priest et al., 2009).

Because so much methane is required to form hydrate, segregated hydrates (Figures 1(v)–1(viii)) require significant upward flow of methane gas into the hydrate stability zone, and are grain displacing. CT scanning of natural hydrate-bearing sediments from pressure cores (Rees et al., 2011) has produced images very similar to the sheet hydrate sketched in Figure 1(v). The steeply dipping and often thin hydrate sheets probably result from hydraulic fracture. In contrast, bedded hydrates (Figure 1(vi)) probably result from the presence of permeable subhorizontal layers within the host sediment (Holland et al., 2008; Kubo et al., 2014). These become progressively less permeable as disseminated hydrate is formed within them. Nodular hydrates (Figure 1(vii)) may be associated with burrows and boring of benthos within the seabed sediment as has been observed in other sediment types (Kennedy & Garrison, 1975). Because of the reduced proportion of host sediment per unit volume, bedded, nodular, and massive hydrate-bearing sediments can be expected to have strength and stiffness properties that approach those of solid methane hydrate.

3. Mechanisms Leading to Strength and Stiffness Change During Hydrate Formation and Dissociation

Because of the varying hydrate morphology described above, and degree of hydrate saturation, the effects of hydrate formation and dissociation on the strength and stiffness of young seafloor sediment can be expected to be extremely variable. A number of sediment softening/weakening mechanisms have been postulated:

1. Increase or reduction of strength due to changes in intergranular contact cementation (Figure 1(iv); Yoneda et al., 2016);
2. Change in pore space (void ratio) by removal of hydrate (Figures 1(i), 1(ii), and 1(vi)–1(viii));
3. Reduction of effective stress, perhaps leading to hydraulic fracture in fine-grained sediments, as pore fluid (gas) pressure increases during dissociation;
4. Removal of overburden-supporting subvertical hydrate sheets (Figure 1(v)), in soft, fine-grained host sediment (Kubo et al., 2014; Rees et al., 2011); and
5. Change in the plasticity of the sediment as progressive destructuring takes place, releasing freshwater from the hydrate (Priest et al., 2014).

The work described in this paper explores the effects of mechanism #1 above in stiffening or strengthening the host sediment. The effects of mechanism #1 and #3 on very small strain stiffness have recently been reported by Priest et al. (2014), Sultaniya et al. (2015), and Sultaniya et al. (2017).

Deposits of hydrate have generally been observed in the field in high-permeability sandy sediments. There appear to have been only a few laboratory studies of the effect of host sediment properties such as grain size and sphericity, on stiffness (Clayton et al., 2010; Waite et al., 2004), and strength (Hyodo et al., 2013; Masui et al., 2005; Miyazaki et al., 2011; Winters et al., 2007). This study presents the effects of hydrate formation on the host sediment stiffness and strength. It can be expected that any increase in material properties as a result of hydrate formation will be reversed during dissociation (Priest et al., 2005). In reality, it seems likely that the strength of the host sediment after hydrate formation and dissociation may be lower than its original value, as a result of destructuring.

4. Temperature-Controlled Triaxial Apparatus

To investigate the effect of contact cementation on the mechanical properties of gas hydrate-bearing granular sediments, specimens were artificially formed within the pore space of four different granular (sand-sized) materials, and sheared using a gas hydrate triaxial apparatus. Descriptions of the apparatus, materials, and the test methods are outlined below.

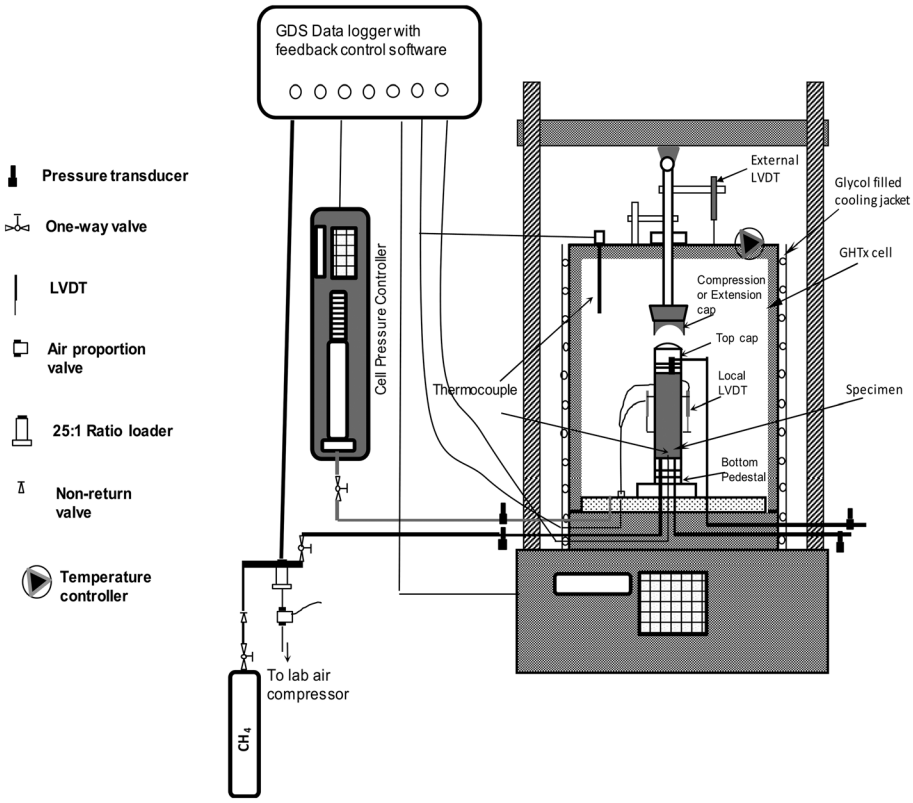

Figure 2. Gas hydrate triaxial apparatus.

The gas hydrate triaxial apparatus contained a tailor-made high-pressure cell capable of applying a pressure of up to 20 MPa and of controlling the specimen temperature between +50 °C and −20 °C to ±0.5 °C. Ethylene glycol was used both as the cell fluid and recirculating fluid for an in-cell heat-exchange coil. A schematic diagram of the apparatus is shown in Figure 2. The whole apparatus was surrounded by thermal jackets in order to further improve temperature control. The apparatus was equipped with an internal load cell, pore pressure transducer, internal thermistor, and linear variable differential transformers to measure the local deformation and thereby monitor and measure the mechanical response during the process of hydrate formation and subsequent shearing. The pressure transducers and load cell were calibrated using a Budenberg dead weight tester, while the deformation transducers were calibrated using a micrometer.

5. Granular Materials Selected for Testing

Three uniform granular materials were combined in different proportions to explore the effects of dry density, specific surface area, particle shape, and form on stiffness and compressive strength. The materials used were Leighton Buzzard grade B, Leighton Buzzard grade E, and 100 mesh muscovite mica; their physical

Table 1
Properties of the Specimens Tested

Material	Specific Surface Area (m^2/m^3)	Void Ratio of Sand Without Hydrate	Void Ratio of Sand With Hydrate	Water Content (%)	Hydrate Saturation of Sand (%)
LBB	8,000	0.55	0.57	2.29	13.4
LBE	112,000	0.69	0.67	2.49	12.3
LBB/E	18,000	0.52	0.53	1.93	12.5
LBB/M	124,000	0.53	0.49	2.33	15.8

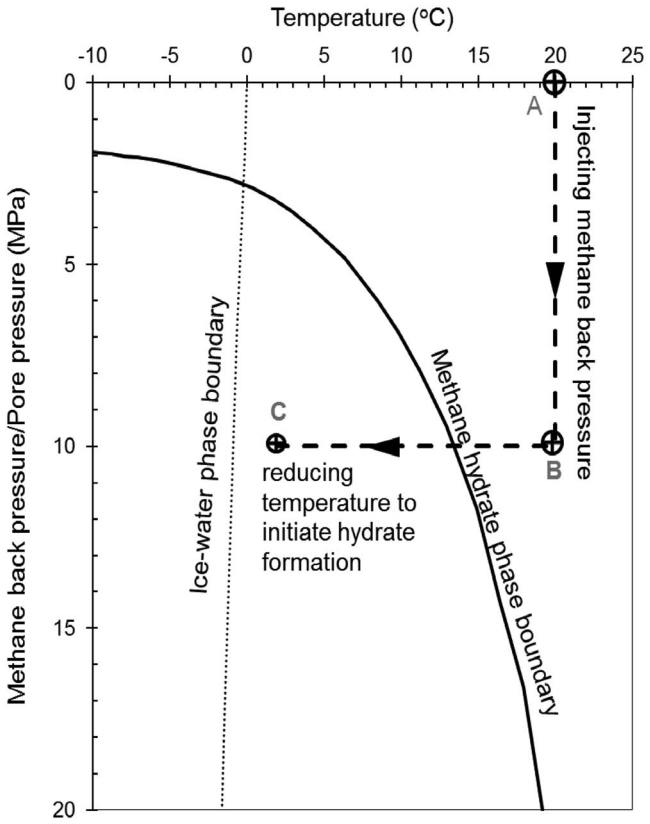

Figure 3. Thermobaric path used for hydrate formation.

properties are described in Clayton et al. (2010), who reported small-strain stiffness tests on them, obtained using the resonant column apparatus. Four different mixtures were tested:

1. 100% Leighton Buzzard grade B (LBB),
2. 100% Leighton Buzzard grade E (LBE),
3. 90% Leighton Buzzard grade B + 10% by weight Leighton Buzzard grade E (LBB/E), and
4. 90% Leighton Buzzard grade B + 10% by weight mica (LBB/M).

LBB has a relatively large grain size ($D_{50} \approx 1.020$ mm) when compared with LBE ($D_{50} \approx 0.120$ mm). Both have high sphericity (Clayton et al., 2009) bulky particles, but LBB's grains are relatively smooth when compared with the more angular LBE (see Clayton et al., 2010, Figures 2 and 3). The 0.085-mm muscovite particles are flat and plate like. The decision to use 10% fines in mixtures (c) and (d) was made in order to increase the specific surface area without allowing the fines to dominate the mechanical behavior of the mixes (Clayton et al., 2004; Georgiannou, 2006; Thevanayagam, 1998).

The physical and geotechnical properties of the eight specimens formed from the three materials and conducted with and without hydrate formation are presented in Table 1. Pairs of specimens were tested, and as can be seen, there were minor, probably insignificant, differences in void ratios between specimens with and without hydrate.

6. Formation of Disseminated Hydrate in Sand

Eight cylindrical specimens, 70-mm diameter and 140 mm in height, were formed. The masses of dry sand required to achieve the target dry densities, based on a previous study (Clayton et al., 2010), were mixed with a mass of water necessary to reach the target hydrate saturations. The moist sands were left overnight in sealed bags, and were then compacted in a three-part split mold using the moist-tamping method (Ladd, 1978). Care was taken to ensure that no spillage of the sand particles occurred and the specimens were wrapped in butyl membranes in order to avoid any gas diffusion at high pressures.

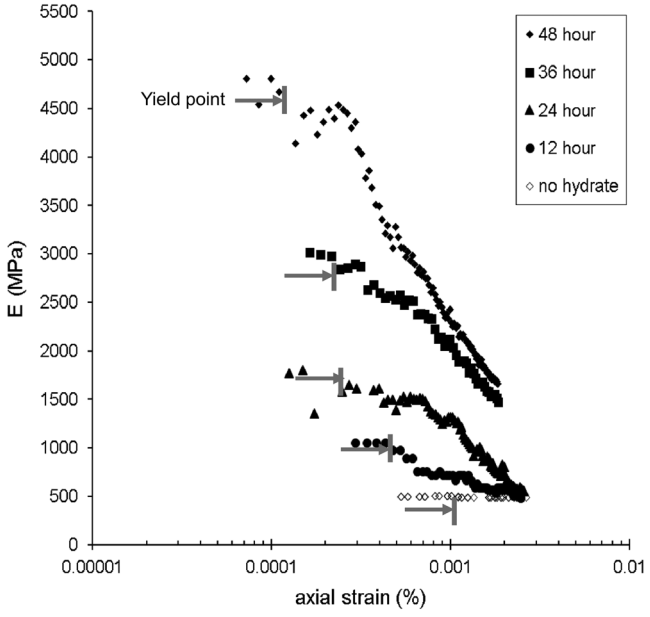

Figure 4. Stiffness of LBB + 10% mica sand during hydrate formation from probing tests. Arrows indicate evolution of yield points.

After sealing, suction was applied to the base pedestal using a vacuum pump, the split mold was removed, and the linear variable differential transformers were fixed to the membrane. The initial void ratios, water contents, and computed degrees of hydrate saturation for the four different granular specimens are given in Table 1. The water content, and therefore the degree of hydrate saturation, was selected because previous tests to determine stiffness (Clayton et al., 2010) had demonstrated that this was sufficient to produce fully cemented specimens (i.e., specimens whose very small strain stiffness was unaffected by the effective stresses applied to them), and also helped maintain an even distribution of water within the sediment (Kumar & Madhusudhan, 2012).

An effective cell pressure of 250 kPa was applied. Methane was injected at 20 °C up to a back pressure of 10 MPa (point A to B; Figure 3) with an effective stress of approximately 250 kPa being maintained, before cooling to 2 °C to form hydrate (point B to C; Figure 3). Temperature, cell pressure, and back pressure were maintained at point C for at least 48 hr to encourage complete hydrate formation. The hydrate content for each specimen (see Table 1) was calculated using equation (1), assuming that all the water in the sand had been converted to hydrate at a molar ratio of methane to water of 1:5.75 (Koh & Sloan, 2007; Priest et al., 2005; Sultaniya et al., 2015).

Table 2
Young's Modulus and Threshold Strain Values of Four Granular Materials Obtained From Probing Tests During the Hydrate Formation Process

	LBB		LBE		LBB + 10% LBE		LBB + 10% Mica	
Time	E (GPa)	$\varepsilon_e \times 10^{-4}$ (%)	E (GPa)	$\varepsilon_e \times 10^{-4}$ (%)	E (GPa)	$\varepsilon_e \times 10^{-4}$ (%)	E (GPa)	$\varepsilon_e \times 10^{-4}$ (%)
12 hr	0.84	-	0.51	-	0.62	-	0.48	-
24 hr	2.03	44.5	1.40	2.0	2.75	9.5	1.14	6.0
36 hr	5.01	30.0	3.70	1.6	6.23	2.5	2.43	1.3
48 hr	6.53	21.5	5.81	1.2	6.90	2.3	4.48	0.9

$$S_h = \frac{m_w \times M_{hy}}{5.75 \times M_w \times \rho_{hy} \times n \times V_t} \quad (1)$$

where m_w is the mass of the added water, M_{hy} is the molar mass of methane hydrate (119.63 g/mol), M_w is the molar mass of water (18.015 g/mol), ρ_{hy} is the mass density of methane hydrate (0.917 g/m^3), n is the porosity of the specimen, and V_t is the sample volume (m^3).

The calculated hydrate contents for each of the different sands hosting hydrates are presented in Table 1.

7. Loading Tests

Three types of loading tests were performed in the gas hydrate triaxial loading apparatus:

1. The evolution of stiffness with time in hydrate-cemented sands was explored by performing multistage undrained small-strain probing tests (Malandraki & Toll, 2000);
2. Following this, stiffnesses were determined under small-scale monotonic loading, using data from the local strain instrumentation; and
3. Finally, the strength of the various hydrate/sand specimens was determined by taking them to failure in triaxial compression.

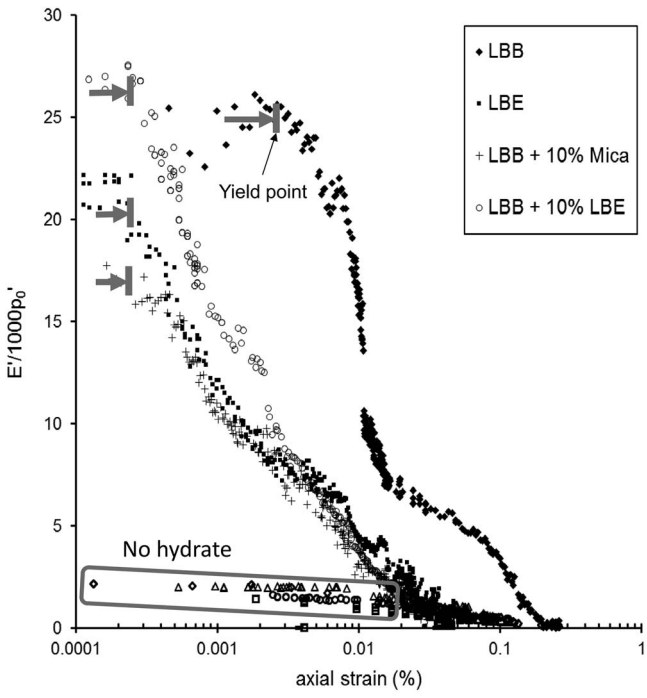

Figure 5. Normalized stiffness evolution of sands with and without hydrate cement. Arrows indicate yield points for different hydrate-bearing sands.

7.1. Probing Tests: Increase of Stiffness With Time

Once the desired specimen temperature, cell pressure, and back pressure had been held for 48 hr (point C; Figure 3), automated displacement-controlled undrained "probing tests" were performed at ≈12-hr intervals, in order to capture the evolution of stiffness during the hydrate formation process. Testing was carried out under an isotropic effective confining stress of 250 kPa. An axial displacement rate equivalent to a global rate of strain of 0.05% per hour was used. After each loading excursion reached an axial strain of 0.01%, or an increase in pore pressure was observed, specimens were unloaded until the deviatoric stress was of the order of 1.5 kPa, which was the applied throughout the triaxial testing in order to maintain contact between the loading ram and specimen top cap, thus avoiding potential problems due to lack of load cell/top cap alignment within the initial part of the stress strain curve.

Figure 4 shows the result of four probing tests for the LBB + 10% mica specimen. Table 2 presents the changes in Young's modulus over time and the associated threshold elastic strain for the four sands used in the study. The results show that specimen stiffness continued to rise between 36 and 48 hr after the start of hydrate formation; there was a reduction in the elastic threshold strain. This suggests that the effects of hydrate on the strength and stiffness values obtained from 12- and 24-hr probe testing may have been underestimated, since the full evolution of strength

Table 3
Small-Strain Stiffness Data From Present Work in Comparison With Resonant Column Data of Clayton et al. (2010)

	E (GPa), Present Study	*E* (GPa), Clayton et al. (2010)	*G* (GPa), Clayton et al. (2010)
LBB	6.53	6.52	3.42
LBE	5.81	5.52	2.68
LBB + 10% LBE	6.90	6.30	3.57
LBB + 10% mica	4.48	4.20	2.51

might have been incomplete at the time of making the measurements. This is in contrast to the findings of Sultaniya et al. (2015, 2017), who observed complete hydrate formation and near-constant stiffness within 12 hr of commencing formation, but is similar to the observations of Rees (2009). It may be the result of Oswald ripening effects (Chaouachi et al., 2017).

7.2. Very Small Strain Stiffness of Hydrate-Cemented Sand

Tangent local Young's moduli were calculated from the stress strain responses of the four granular materials with and without hydrate. The

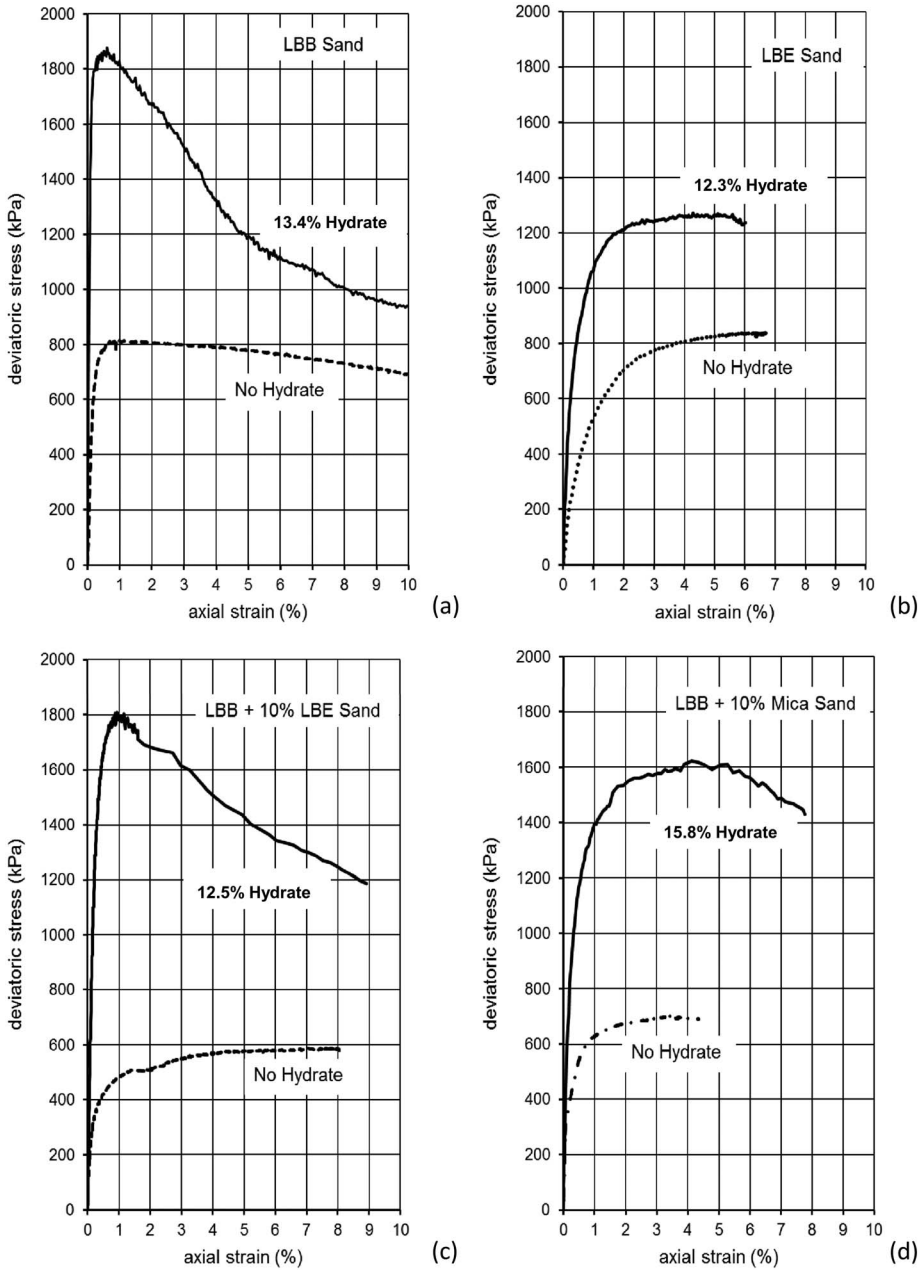

Figure 6. Deviator stress versus linear local axial strain results, with and without hydrate cementing. (a) LBB, (b) LBE, (c) LBB + 10%, and (d) LBB + 10% mica.

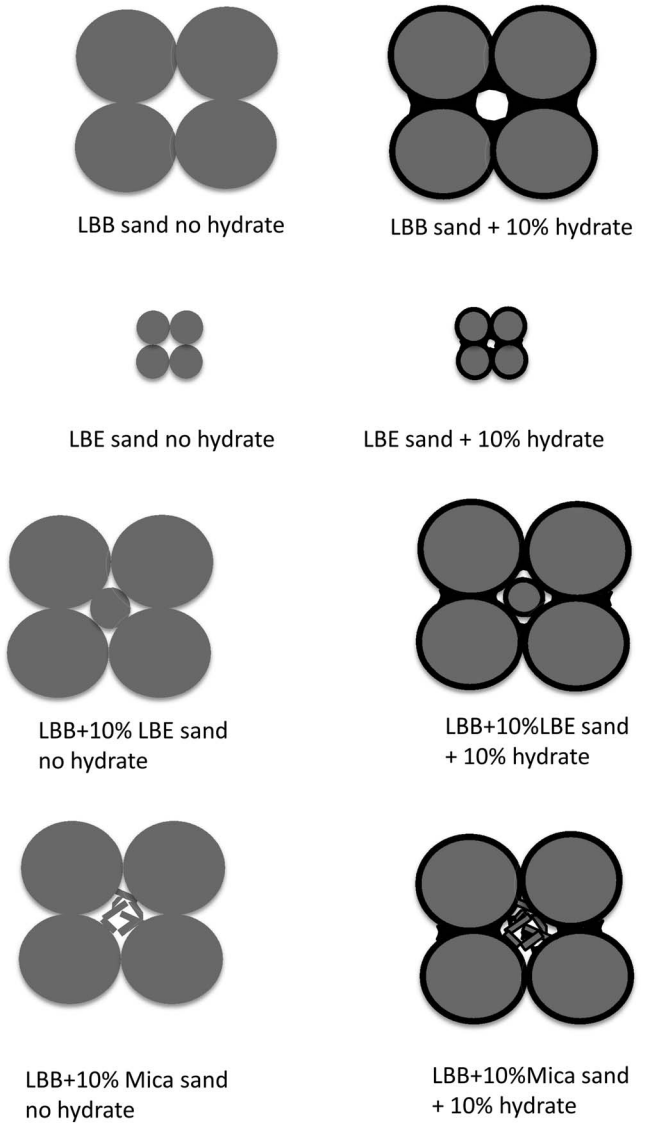

Figure 7. Conceptual sketch visualizing particle arrangement and cemented hydrate within pore space for the four granular material.

Young's moduli, normalized by 1,000 p'_0 (where p'_0 is the initial mean effective stress), are compared in Figure 5. Initial moduli obtained at very small strain levels are similar to those calculated from Resonant Column data for the same four sediments as reported by Clayton et al. (2010) and shown in Table 3. The modulus degradation curves indicate that the particle size, shape, and specific surface area play a significant role not only in the materials' initial stiffness but also in the stiffness degradation once the elastic strain threshold, marked by arrows, is exceeded. Considering particle size, the coarser grained LBB sand yielded from elastic to nonlinear elastic behavior at a strain level of about 4×10^{-3}%, whereas the fine-grained LBE sand yielded at 1 order of strain magnitude less, 2.5×10^{-4}%.

Considering particle shape, LBB + 10% LBE sand had a higher modulus when compared to the LBB + 10% mica at all strain levels, but the yield strain was of a similar order. With respect to the effect of specific surface area, hydrate-bearing LBB sand and LBB + 10% LBE sand exhibit greater stiffness at all strain levels in comparison to higher specific surface area.

7.3. Effect of Hydrate on Strength

Confined triaxial compressive strength tests were carried out under drained conditions on hydrate-bearing specimens approximately 48 hr after the end of probing. The applied rate of axial strain was initially 0.05% per hour, increasing to 0.5% per hour after reaching 0.1% global strain. This rate was then held until the end of test. Figure 6 shows the drained triaxial compression stress–strain curves for each of the four materials, with and without methane hydrate, using the internal load cell and local axial displacement measuring system, under an isotropic effective stress of 250 kPa. The results show that the specimens without hydrate, despite the differences in particle size, shape, and surface roughness, all had quite similar strengths varying between 0.59 and 0.84 MPa.

The measured compressive strengths without hydrate are a function of the effective stress (250 kPa) applied during the tests, which even for a bulk unit weight as high as 20 kN/m^3 would be equivalent to a sediment depth in excess of 25 m. Table 3 shows that the baseline test results have effective angles of friction, φ', of between 32.8° and 38.8°, which are typical values for sands. Assuming for simplicity a linear relationship between strength and effective confining pressure, it can be calculated that at a depth of 10 m below the seabed, the measured confined compressive strength would be much less, of the order of 0.24 to 0.34 MPa. The strengthening effect of disseminated hydrate, as a proportion of the uncemented compressive strength, would therefore be much greater at shallow depths. The stress–strain behavior of the materials with 13–16% hydrate is markedly different to those without hydrate. The confined compressive strength after hydrate formation varies from 1.28 to 1.86 MPa. Considering particle size effects (Figures 6a and 6b), specimens with hydrate-bearing coarse sand (LBB; d_{50}~1.0 mm) exhibit distinct peaks and strain-softening behavior, in comparison to fine sand (LBE; d_{50}~0.1 mm) which shows a strain-hardening behavior, at least up to 5% axial strain.

Considering the specific surface area of the particles (Table 1), hydrate-bearing LBB sand and LBB + 10% LBE sand have a low specific surface area and exhibit distinct peak and strain-softening behavior (Figures 6a and 6c). This is in contrast with the strain-hardening behavior exhibited by hydrate-bearing sand with ~7 to 10 times more specific surface area, LBE and LBB + 10% mica sand (Figures 6b and 6d). This may be an indication that the amounts of hydrate formed in these tests (12.3% and 15.8% hydrate saturation) were insufficient to fully cement them, that is, to make their strengths independent of the applied effective stress. Particle form similarly affects the strength behavior of hydrate cemented sediments. Changing the particle form of the secondary constituent from subrounded to platy modified the behavior from strain softening to a strain hardening one, at least up to about 5% strain (Figures 6c and 6d). Figure 7 presents conceptual sketch of particle

Table 4
Strengths of the Four Host Materials, With and Without Hydrate Cement

Host Material	Confined Compressive Strength of Uncemented Host Material (MPa)	Confined Compressive Strength of Host Material Plus Hydrate Cement (MPa)	Strength Changes Caused by Dissociation of Hydrate (%)		Drained Peak Friction Angle ϕ' (deg)	Reduction in Cohesion Caused by Hydrate Dissociation (kPa)
			Calculated Strength Change	Measured Strength Change		
			σ' = 100 kPa	σ' = 250 kPa		
LBB	0.81	1.86	82.6	56.5	38.2	255
LBE	0.84	1.28	73.8	34.4	38.8	105
LBB + 10% LBE	0.59	1.80	86.9	67.2	32.8	330
LBB + 10% mica	0.70	1.62	82.7	56.8	35.7	236

arrangement and hydrate cementation within pore space for the four granular sediments to visualize the difference in the sediment pore-scale structure. Table 4 gives the peak strengths of the specimens, with and without methane hydrate.

To interpret the triaxial strength data, a simple Mohr-Coulomb (c', φ') model was adopted. The effective angle of friction of each uncemented material was calculated from the confined compressive strengths of the host materials assuming, because of the low degrees of saturation of the specimens, no generation of excess pore pressure during shear. In this simple model the effective cohesion intercept is conventionally taken as zero for uncemented sand. The effective cohesion intercept of cemented sand is back-figured, assuming that the effective angle of friction of the host material is unaffected by cementation (Waite et al., 2009), following (for example) the approach for unsaturated soils adopted for by Lu and Likos (2006). On this basis the triaxial test data can be interpreted as in Figure 6. The loss of strength due to dissociation can be judged from Figure 8 and the data given in Table 4.

Sands tested under an effective confining pressure of 250 kPa in the absence of hydrates had strengths of the order of 35–70% lower than when hydrate was present. In the case of LBB + 10% LBE, there was an ~67% reduction in peak strength between the hydrate- and nonhydrate-bearing specimens. These values would be proportionately larger for specimens at the lower effective stress levels (Table 3) typically encountered at submarine slope failures. Particle size plays a significant role in determining the impact of hydrate on the strength of an unsaturated host sediment, where cemented hydrate is deposited primarily at contact points. A very large reduction in cohesion intercept ($>$ 200 kPa) was observed for the coarser LBB sediments in comparison to fine LBE sand (95 kPa). Particle form had a significant effect on the reduction of the cohesion

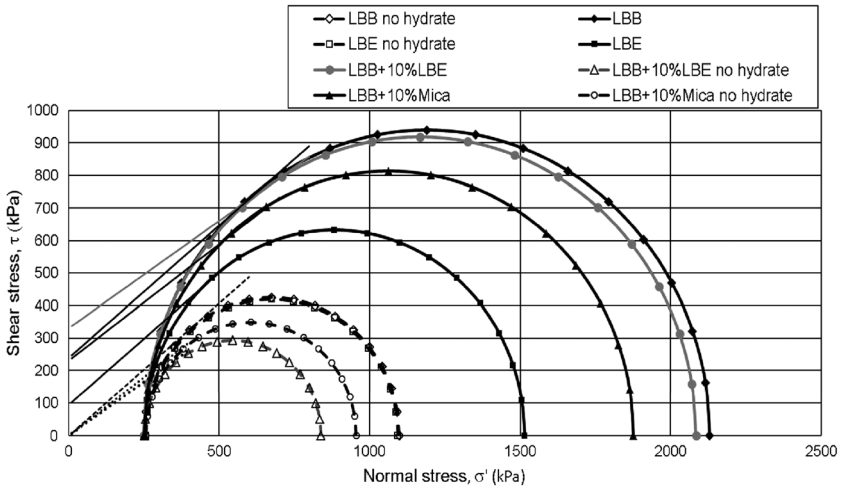

Figure 8. Comparison of sands with and without gas hydrate cement, using Mohr's circles.

component; greater strength loss was observed for subrounded secondary constituents in comparison to platy ones, perhaps as a result of particle flexing under load.

8. Conclusions

This paper reports the results of laboratory testing to evaluate the effects of gas hydrate dissociation on the stiffness and strength of hydrate-bearing sands. The effects of hydrate cementation have been studied for a range of granular materials with differing specific surface areas and particle shapes, using a bespoke laboratory gas hydrate triaxial apparatus. In contrast with the findings of Sultaniya (2011), our probing tests suggest that disseminated hydrate triaxial specimens made using the excess gas technique should be left to stand for at least 36–48 hr before testing begins. The change in strength and stiffness reported in this paper as a result of hydrate formation are probably conservative.

Stiffnesses obtained at small strain from the locally instrumented triaxial tests reported here are close to those reported by Clayton et al. (2010), obtained from resonant column testing. These results give confidence in the observation that at very small strain a tenfold increase in stiffness can be expected. Degradation in stiffness under triaxial conditions appeared to take place more slowly (as a function of strain) in coarse uniform sands than in finer materials.

The strength gain in cemented hydrate-bearing sediments depends strongly on particle specific surface area, size, and form. Particles with higher specific surface area and smaller average grain size exhibit strain-softening behavior, in comparison to the strain-hardening behavior of particles with much lower specific surface area and bigger particle size. Given similar effective stress and hydrate content, the gain in strength due to hydrate cementation is ~1.6 times higher for LBB sand in comparison to LBE sand. Similarly, comparing the gain in cementation with regard to specific surface area or particle form, particle size seems to have a significant influence on the strength of host granular materials.

Under triaxial compression conditions, yield of hydrate cemented sand is particle size dependent. Stiffness also appears to be dependent on specific surface area of the material; higher stiffness was found for lower specific surface area material. The change of strength/stiffness for lower specific surface area, larger particle size hydrate-cemented granular sediments is very large when hydrate forms, and would suggest a rapid loss in strength if hydrate dissociates. On the other hand, higher specific surface area and smaller particle size sediments may lose strength progressively under thermobaric changes as the yield occurs early at lower strains compared to sediments of lower specific area and larger particle size.

Acknowledgments
This research work was supported by the NERC Arctic Research Programme assessing the impact of climate change on the landslide–tsunami risk to the UK (NE/K00008X/1). The associated data are available in the supporting information and at the National Geoscience Data Centre, UK (www.bgs.ac.uk/services/NGDC/home.html).

References

Chaouachi, M., Neher, S. H., Falenty, A., & Kuhs, W. F. (2017). Time resolved coarsening of clathrate crystals: The case of gas hydrates. *Crystal Growth and Design*, *17*(5), 2458–2472. https://doi.org/10.1021/acs.cgd.6b01875

Clayton, C. R. I. (2011). Stiffness at small strain: Research and practice. *Géotechnique*, *61*(1), 5–37. https://doi.org/10.1680/geot.2011.61.1.5

Clayton, C. R. I., Abbireddy, C. O. R., & Schiebel, R. (2009). A method of estimating the form of coarse particulates. *Géotechnique*, *59*(6), 193–501. https://doi.org/10.1680/geot.2007.00195

Clayton, C. R. I., Priest, J. A., & Best, A. I. (2005). The effects of disseminated methane hydrate on the dynamic stiffness and damping of a sand. *Géotechnique*, *55*(6), 423–434. https://doi.org/10.1680/geot.2005.55.6.423

Clayton, C. R. I., Priest, J. A., & Rees, E. V. L. (2010). The effects of hydrate cement on the stiffness of some sands. *Géotechnique*, *60*(6), 435–445. https://doi.org/10.1680/geot.2010.60.6.435

Clayton, C. R. I., Theron, M., & Best, A. I. (2004). The measurement of vertical shear-wave velocity using side-mounted bender elements in the triaxial apparatus. *Géotechnique*, *54*(7), 495–498. https://doi.org/10.1680/geot.2004.54.7.495

Dvorkin, J., Helgerud, M. B., Waite, W. F., Kirby, S. H., & Nur, A. (2000). Introduction to physical properties and elasticity models. In M. D. Max (Ed.), *Natural Gas Hydrate in Oceanic and Permafrost Environments* (Chap. 20, pp. 245–260). Netherlands: Kluwer Academic Publishers.

Ecker, C., Dvorkin, J., & Nur, A. (1998). Sediments with gas hydrates: Internal structure from seismic AVO. *Geophysics*, *63*(5), 1659–1669. https://doi.org/10.1190/1.1444462

Georgiannou, V. N. (2006). The undrained response of sands with additions of particles of various shapes and sizes. *Géotechnique*, *56*(9), 639–649. https://doi.org/10.1680/geot.2006.56.9.639

Holland, M., Schultheiss, P., Roberts, J. and Druce, M. (2008). Observed gas hydrate morphologies in marine sediments. Proceedings of the 6th International Conference on Gas Hydrates (ICGH 2008), CANADA.

Hyodo, M., Yoneda, J., Yoshimoto, M., & Nakata, Y. (2013). Mechanical and dissociation properties of methane hydrate-bearing sand in deep seabed. *Soils and Foundations*, *53*(2), 299–314. https://doi.org/10.1016/j.sandf.2013.02.010

Kennedy, W. J., & Garrison, R. E. (1975). Morphology and genesis of nodular chalks and hardgrounds in the upper Cretaceous of southern England. *Sedimentology*, *22*(3), 311–386. https://doi.org/10.1111/j.1365-3091.1975.tb01637.x

Koh, C. A., & Sloan, E. D. (2007). Natural gas hydrates: Recent advances and challenges in energy and environmental applications. *AICHE Journal*, *53*(7), 1636–1643. https://doi.org/10.1002/aic.11219

Kubo, Y., Mizuguchi, Y., Inagaki, F., & Yamamoto, K. (2014). A new hybrid pressure-coring system for the drilling vessel Chikyu. *Scientific Drilling*, *17*, 37–43. https://doi.org/10.5194/sd-17-37-2014

Kumar, J., & Madhusudhan, B. N. (2012). Dynamic properties of sand from dry to fully saturated states. *Géotechnique*, *62*(1), 45–54. https://doi.org/10.1680/geot.10.P.042

Kvalstad, T. J., Andresen, L., Forsberg, C. F., Berg, K., Bryn, P., & Wangen, M. (2005). The Storegga slide: Evaluation of triggering sources and slide mechanics. *Marine and Petroleum Geology*, *22*(1-2), 245–256. https://doi.org/10.1016/j.marpetgeo.2004.10.019

Ladd, R. S. (1978). Preparing test specimens using under-compaction. *Geotechnical Testing Journal*, *1*(1), 16–23.

Lu, N., & Likos, W. J. (2006). Suction stress characteristic curve for unsaturated soil. *Journal of Geotechnical and Geoenvironmental Engineering, ASCE*, *132*(2), 131–142.

Madhusudhan, B. N., Clare, M. A., Clayton, C. R. I., & Hunt, J. E. (2017). Geotechnical profiling of deep-ocean sediments at the AFEN submarine slide complex. *Quarterly Journal of Engineering Geology and Hydrogeology*, *50*(2), 148–157. https://doi.org/10.1144/qjegh2016-057

Malandraki, V., & Toll, D. (2000). Drained probing triaxial tests on a weakly bonded artificial soil. *Géotechnique*, *50*(2), 141–151. https://doi.org/10.1680/geot.2000.50.2.141

Malone, R. (1985). Gas Hydrates Topical Report (Department of Energy, Morgantown Energy Technology Center, USA) DOE/METC/SP-218 (DE85001986).

Masui, A., Haneda, H., Ogata, Y., & Aoki, K. (2005). The effect of saturation degree of methane hydrate on the shear strength of synthetic methane hydrate sediments. In *5th International Conference on Gas Hydrates* (pp. 657e663). Trondheim, Norway.

Miyazaki, K., Masui, A., Sakamoto, Y., Aoki, K., Tenma, N., & Yamaguchi, T. (2011). Triaxial compressive properties of artificial methane-hydrate-bearing sediment. *Journal of Geophysical Research*, *116*, B06102. https://doi.org/10.1029/2010JB008049

Mountjoy, J. J., Pecher, I., Henrys, S., Crutchley, G., Barnes, P. M., & Faverola, P. A. (2014). Shallow methane hydrate system controls ongoing, downslope sediment transport in a low-velocity active submarine landslide complex, Hikurangi margin, New Zealand. *Geochemistry, Geophysics, Geosystems*, *15*, 4137–4156. https://doi.org/10.1002/2014GC005379

Priest, J. A., Best, A. I., & Clayton, C. R. I. (2005). A laboratory investigation into the seismic velocities of methane gas hydrate-bearing sand. *Journal of Geophysical Research*, *110*, B04102. https://doi.org/10.1029/2004JB003259

Priest, J. A., Clayton, C. R. I., & Rees, E. V. L. (2014). Potential impact of gas hydrate and its dissociation on the strength of host sediment in the Krishna-Godavari Basin. *Marine and Petroleum Geology*, *523*(58), 187–198.

Priest, J. A., Rees, E. V. L., & Clayton, C. R. I. (2009). Influence of gas hydrate morphology on the seismic velocities of sands. *Journal of Geophysical Research*, *114*, B11205. https://doi.org/10.1029/2009JB006284

Rees, E. V. L., Priest, J. A., & Clayton, C. R. I. (2011). The structure of methane gas hydrate bearing sediments from the Krishna-Godavari Basin as seen from micro-CT scanning. *Marine and Petroleum Geology*, *28*(7), 1283–1293. https://doi.org/10.1016/j.marpetgeo.2011.03.015

Rees, E. V. L. (2009). Methane gas hydrate morphology and its effect on the stiffness and damping of some sediments, (Doctoral thesis, 207 pp.). University of Southampton, School of Civil Engineering and the Environment.

Rydzy, M. B. (2014). The effect of hydrate formation on the elastic properties of unconsolidated sediment, (PhD thesis, pp. 127). Colorado School of mines.

Song, Y., Yu, F., Li, Y., Liu, W., & Zhao, J. (2010). Mechanical property of artificial methane hydrate under triaxial compression. *Journal of Natural Gas Chemistry*, *9*(3), 246–250.

Sultaniya, A. K., Priest, J. A., & Clayton, C. R. I. (2015). Measurements of the changing wave velocities of sand during the formation and dissociation of disseminated methane hydrate. *Journal of Geophysical Research: Solid Earth*, *120*, 778–789. https://doi.org/10.1002/2014JB011386

Sultaniya, A. K., Priest, J. A., & Clayton, C. R. I. (2017). The impact of formation and dissociation on the stiffness of a hydrate bearing sand. *Canadian Geotechnical Journal*, *55*(7), 988–998. https://doi.org/10.1139/cgj-2017-0241

Talling, P., Clare, M., Urlaub, M., Pope, E., Hunt, J. E., & Watt, S. (2014). Large submarine landslides on continental slopes: Geohazards, methane release, and Climate Change. *Oceanography*, *27*(2), 32–45.

Thevanayagam, S. (1998). Effect of fines and confining stress on undrained shear strength of silty sands. *Journal of Geotechnical and Geoenvironmental Engineering, ASCE*, *124*(6), 479–491.

Waite, W. F., Santamarina, J. C., Cortes, D. D., Dugan, B., Espinoza, D. N., Germaine, J., Jang, J., et al. (2009). Physical properties of hydrate-bearing sediments. *Reviews of Geophysics*, *47*, RG4003. https://doi.org/10.1029/2008RG000279

Waite, W. F., Winters, W. J., & Mason, D. H. (2004). Methane hydrate formation in partially water saturated Ottawa sand. *American Mineralogist*, *89*(8–9), 1202–1207. https://doi.org/10.2138/am-2004-8-906

Winters, W. J., Waite, W. F., Mason, D. H., Gilbert, L. Y., & Pecher, I. A. (2007). Methane gas hydrate effect on sediment acoustic and strength properties. *Journal of Petroleum Science and Engineering*, *56*(1-3), 127–135. https://doi.org/10.1016/j.petrol.2006.02.003

Yelisetti, S., Spence, G. D., & Riedel, M. (2014). Role of gas hydrates in slope failure on frontal ridge of northern Cascadia margin. *Geophysical Journal International*, *199*, 441–458.

Yoneda, J., Jin, Y., Katagiri, J., & Tenma, N. (2016). Strengthening mechanism of cemented hydrate-bearing sand at microscales. *Geophysical Research Letters*, *43*, 7442–7450. https://doi.org/10.1002/2016GL069951

Yu, F., Song, Y., Liu, W., Li, Y., & Lam, W. H. (2011). Analyses of stress strain behaviour and constitutive model of artificial methane hydrate. *Journal of Petroleum Science and Engineering*, *77*(2), 183–188. https://doi.org/10.1016/j.petrol.2011.03.004